Poly(sodium 4-styrenseulfonate)-modified monolayer graphene for anode applications of organic photovoltaic cells

Yongfang Zhou, Min Wang, Liang Wang, Shuli Liu, Shufen Chen, Kun Cao, Wenjuan Shang, Jiangquan Mai, Baomin Zhao, Jing Feng, Xinhui Lu, and Wei Huang

Citation: Appl. Phys. Lett. **111**, 113302 (2017);

View online: https://doi.org/10.1063/1.5003348

View Table of Contents: http://aip.scitation.org/toc/apl/111/11

Published by the American Institute of Physics

Articles you may be interested in

Decoupling degradation in exciton formation and recombination during lifetime testing of organic light-emitting devices
Applied Physics Letters **111**, 113301 (2017); 10.1063/1.4993618

Low-energy electron excitation effect on formation of graphene nanocrystallites during carbon film growth process
Applied Physics Letters **111**, 114105 (2017); 10.1063/1.4990117

Enhanced p-type behavior in the hybrid structure of graphene quantum dots/2D-WSe_2
Applied Physics Letters **111**, 111603 (2017); 10.1063/1.4989598

Flexible graphene sound device based on laser reduced graphene
Applied Physics Letters **111**, 103104 (2017); 10.1063/1.5002113

Resonant tunneling and multiple negative differential conductance features in long wavelength interband cascade infrared photodetectors
Applied Physics Letters **111**, 113504 (2017); 10.1063/1.4994858

Significant increase of quantum efficiency of green InGaN quantum well by realizing step-flow growth
Applied Physics Letters **111**, 112102 (2017); 10.1063/1.5001185

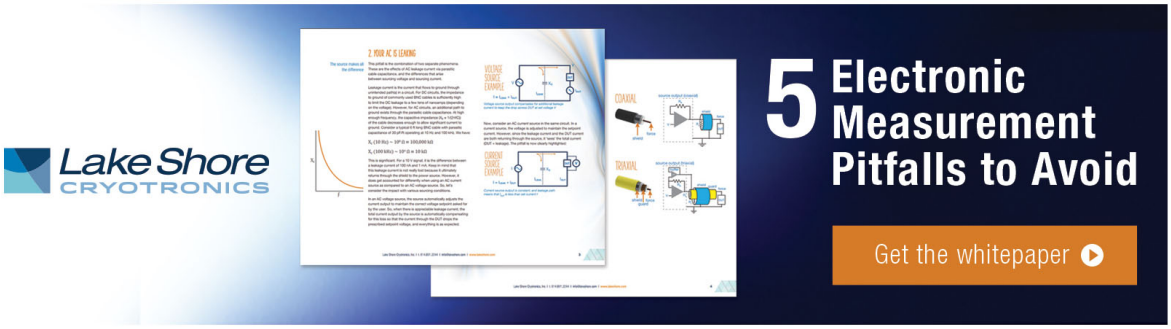

Poly(sodium 4-styrenseulfonate)-modified monolayer graphene for anode applications of organic photovoltaic cells

Yongfang Zhou,[1] Min Wang,[1] Liang Wang,[1] Shuli Liu,[1] Shufen Chen,[1,2,a)] Kun Cao,[1] Wenjuan Shang,[1] Jiangquan Mai,[3] Baomin Zhao,[1,2,a)] Jing Feng,[4] Xinhui Lu,[3,a)] and Wei Huang[1,2,a)]

[1]*Key Laboratory for Organic Electronics and Information Displays and Institute of Advanced Materials (IAM), Jiangsu National Synergetic Innovation Center for Advanced Materials (SICAM), Nanjing University of Posts and Telecommunications (NUPT), 9 Wenyuan Road, Nanjing 210023, China*
[2]*Key Laboratory of Flexible Electronics (KLOFE) and Institute of Advanced Materials (IAM), Jiangsu National Synergetic Innovation Center for Advanced Materials (SICAM), Nanjing Tech University, 30 South Puzhu Road, Nanjing 211816, China*
[3]*Department of Physics, Chinese University of Hong Kong, New Territories, Hong Kong*
[4]*State Key Laboratory on Integrated Optoelectronics, College of Electronic Science and Engineering, Jilin University, Changchun 130012, China*

(Received 27 March 2017; accepted 5 September 2017; published online 15 September 2017)

An insulated poly(sodium 4-styrenseulfonate) (PSS) was used to modify monolayer graphene for anode applications of organic photovoltaics (OPVs). With this PSS interfacial modification layer, the OPVs showed a significant increase of 56.4% in efficiency due to an improved work function and hydrophilic feature of graphene and an enlarged recombination resistance of carriers/excitons. Doping a highly contorted 1,2,5-thiadiazole-fused 12-ring polyaromatic hydrocarbon into the active layer to form ternary blended OPVs further enlarged the recombination resistance of carriers/excitons and improved light absorption of the active layer, with which a high power conversion efficiency of 6.29% was acquired. *Published by AIP Publishing*. [http://dx.doi.org/10.1063/1.5003348]

Organic photovoltaics (OPVs) have attracted enormous attention in recent years due to organic semiconductor's unique features including high absorption coefficients, light weight, low-cost, fine bendability, and compatibility with flexible electronic fabrication processes. In these devices, doped metal oxides such as tin-doped indium oxide (ITO) and fluorine-doped tin oxide (FTO) have been predominantly used as the transparent conducting electrodes. The use of such materials as electrodes may be problematic for organic electronic devices due to the limited indium source on earth, the susceptibility of ion diffusion to organic active layers, and mechanical brittleness of ITO and FTO, especially towards flexible electronics applications. Recently, some novel nanomaterials, e.g., carbon nanotubes,[1,2] graphene,[3,4] and metallic nanowires,[5,6] have been used as transparent electrodes of flexible devices for their ability of withstanding strains of more than 10%, of which graphene as a promising candidate electrode has been extensively studied owing to its high conductivity, excellent transparency, large mechanical compliance, low surface roughness, and perfect flexibility.[3,4]

In previous research work, reduced graphene oxide was mainly employed as the transparent electrode of the OPVs, and relatively low power conversion efficiency (PCE) was obtained due to an extremely high sheet resistance of the graphene film.[7,8] More recently, a significant increase in PCE emerged with successful synthesis of a high conductive chemical vapor deposition (CVD)-deposited graphene film[9,10] although the PCE values based on graphene electrodes were far lower than the counterparts with ITO electrodes.[11–13] For example, Wang *et al*. modified the graphene films with pyrene butanoic acid succinimidyl ester (PBASE) and produced the best performance of 1.71% in poly(3-hexyl)thiophene (P3HT):phenyl-C_{61}-butyric acid methyl ester ($PC_{61}BM$) bulk heterojunction devices. Obvious enhancements from 0.21% with a pristine graphene electrode to 1.71% with the PBASE-modified one were ascribed to an increased work function (WF), an improved hydrophilic property, and a maintained high conductivity of pristine graphene after PBASE noncovalent functionalization.[10] Similarly, interfacial modification to graphene with $AuCl_3$, HNO_3, and MoO_3 also offered OPV performance enhancements by forming a *p*-type doping and thus increasing graphene's WF.[14–16] Wu *et al*. utilized a ferroelectric polymer poly(vinylidene fluoride-co-trifluoroethylene) [P(VDF-TrFE)] to electrostatically dope graphene films and improved PCE from 1.68% to 2.07% in P3HT:$PC_{61}BM$-based devices with 5-layer graphene films.[17] The primary mechanism for performance enhancement is the electrostatic doping-induced decrease in the sheet resistance of graphene films (from 146.15 to 73.6 Ω/sq). It is noticeable that in their configurations of using a single graphene layer, the PCE value was quite low (0.43%) due to a large sheet resistance of graphene up to 421.41 Ω/sq, and it only increased to 1.04% after polarization treatment.

In this paper, we modified the monolayer graphene (MLG) anode with an insulated poly(sodium 4-styrenesulfonate) (PSS) and observed PCE improvements in poly[4,8-bis(5-(2-ethylhexyl)thiophen-2-yl)benzo[1,2-*b*:4,5–*b*′]dithiophene-co-3-fluorothieno[3,4-*b*]thiophene-2-carboxylate]:[6,6]-phenyl-C_{71}-butyric acid methyl ester (PCE-10:$PC_{71}BM$)-based bulk heterojunction OPVs. The concept of using insulating materials for controlling the electrode has been commonly used in OPVs

a)Authors to whom correspondence should be addressed: iamsfchen@njupt.edu.cn; iambmzhao@njupt.edu.cn; xhlu@phy.cuhk.edu.hk; and iamdirector@njupt.edu.cn.

with ITO electrodes[18] but rarely reported in those solar cells using graphene electrodes. Herein, the insulated polymer PSS enhances graphene's WF and then improves PCE by forming dipoles at the interface of the graphene/hole extraction layer, instead of forming a *p*-type doping to graphene. The use of PSS also enlarges the recombination resistance in the solar cells and thus reduces exciton/carrier recombination, followed by significant enhancements of short-circuit current density (J_{sc}), fill factor (FF), and PCE. By further introducing a highly contorted 1,2,5-thiadiazole-fused 12-ring polyaromatic hydrocarbon (DNNBT-C12)[19] into the PCE-10:$PC_{71}BM$ blended active layer to form ternary blended OPVs, a high PCE of 6.29% is acquired due to an increase in the recombination resistance together with an improved light absorption of the active layer.

Graphene films were synthesized with a CVD process using copper (Cu) foils as substrates. A thin layer of poly (methyl methacrylate) (PMMA) was spin-coated onto the Cu foil as a supporting layer, and then, the foil was annealed at 100 °C for 30 min. Subsequently, the Cu foil was etched in a 0.1 M aqueous ammonium persulfate [$(NH_4)_2S_2O_8$] solution.[20] After 12 h, Cu underneath MLG/PMMA was etched away and the graphene was then transferred to a glass substrate, followed by washing with deionized water for three times. After that, the glass-supported graphene film was soaked in acetone for 12 h to sufficiently remove PMMA. Before use, the graphene sheet was cleaned with hot acetone (60 °C) twice and then heated on the hot plate at 120 °C for 20 min. The as-transferred MLG film showed an extremely high transparency in the visible region and is suitable for use as a transparent electrode, as shown in Figs. 1(a) and 1(b) [the photographs and the transmittivity curves]. The optical image of MLG in Fig. 1(c) is continuous without any wrinkle and PMMA residue, indicative of a wonderful quality of our MLG film. The resistance of our pristine graphene sheet is approximately 1 kΩ/sq. Then, a 5×10^{-4} wt. % PSS aqueous solution was spin-coated onto the graphene film to modify the graphene anode prior to OPV fabrication. The as-formed PSS ultrathin layer has a thickness of 0.3 ± 0.05 nm, measured with an Alpha spectroscopic ellipsometer. After PSS coating, the graphene film maintains a high transmittivity of ~96% in the visible range. Fortunately, its contact angle decreases from 88.0° [panel (e)] to 77.5° [panel (f)], indicating an improved hydrophilic feature for the modified graphene surface, which is beneficial for the formation of the uniform polymer films onto graphene via a spin-coating technique. The optical image in panel (d) of Fig. 1 shows a flat and uniform graphene film after PSS modification, similar to the counterpart without any modification [panel (c) of Fig. 1].

Although our statistical results on G- and 2D-bands of Raman spectroscopy [panels (g) and (h) of Fig. 1] may represent a *p*-type doping in the PSS-coated graphene due to obvious blue-shifts in both G- and 2D-bands,[21] X-ray photoelectron spectroscopy (XPS) analysis in Fig. S1 (supplementary material) indicated that the characteristic C1s graphene peak shows no obvious shift towards lower binding energies, and this rules out the possibility of doping.[22] The sheet resistance of up to 1.7 kΩ/sq after PSS modification also demonstrates this point, which is different from the *p*-type doping with a universal decrease in the sheet resistance.[11] To investigate possible influence of the PSS insulator on the interface energy level, the He Iα ultraviolet photoelectron spectroscopy (UPS) spectra of the intrinsic and the PSS-modified graphene were analyzed, as shown in Figs. 2(a) and 2(b). Note that the WF of graphene or the Fermi level of the PSS-coated graphene was calculated by using the photoemission onset to subtract the excitation energy of 21.22 eV. Upon the coating of PSS, the photoemission onset [Fig. 2(a), marked with solid lines] shifted towards a lower binding energy which corresponds to a higher Fermi level (E_F) of 4.68 eV (4.38 eV for pristine graphene). Based on the above analysis, an energy level diagram of PSS-modified graphene was drawn, as shown in Fig. 2(e) [the part in the dashed line box], from which a vacuum level (E_V) bending of ~0.3 eV is observed at the graphene/PSS interface induced by an interfacial dipole, and this level bending helps to reduce barrier for hole extraction.

To verify the influence of dipole on the OPV performances, OPVs were manufactured onto the PSS-modified MLG sheets, with the device configuration and molecular structures of the donor and acceptor shown in Figs. 2(c) and 2(d). The poly(3,4-ethylenedioxythiophene):poly(4-styrenesulfonate) (PEDOT:PSS) buffer layer and the photoactive layer of PCE-10:$PC_{71}BM$ were spin-coated onto PSS in sequence, followed by the thermal deposition of lithium fluoride (LiF) and Al as the electron extraction layer and the cathode. The active area as defined by the overlap of the anode and cathode is 0.1 cm^2. The devices without and with PSS are denoted as devices 1 and 2, while they are termed devices 3 and 4 when introducing a small molecular material DNNBT-C12 into the active layer and forming a ternary blend polymer.

Figure 3(a) shows the current density versus voltage curves of the devices 1–4 under AM 1.5G illumination. Parameters including open-circuit voltage (V_{oc}), J_{sc}, FF, and PCE were extracted into Table I to evaluate the cell

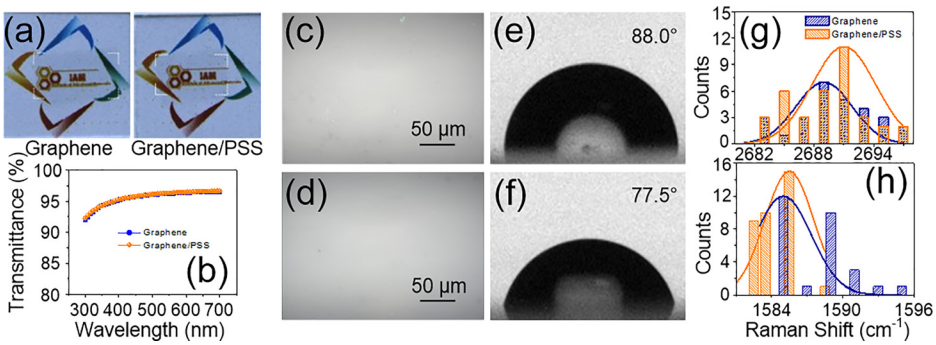

FIG. 1. (a) Photographs of the as-transferred MLG without and with PSS modification. (b) Transmittivity curves of the pristine and PSS-modified graphene sheets. (c) and (d) Optical microscopy images of (c) the pristine graphene film and (d) the modified graphene sheet on Si substrates. (e) and (f) Contact angles of (e) the pristine graphene film and (f) the modified graphene sheet. (g) 2D peak and (h) G peak distribution histogram of Raman spectra.

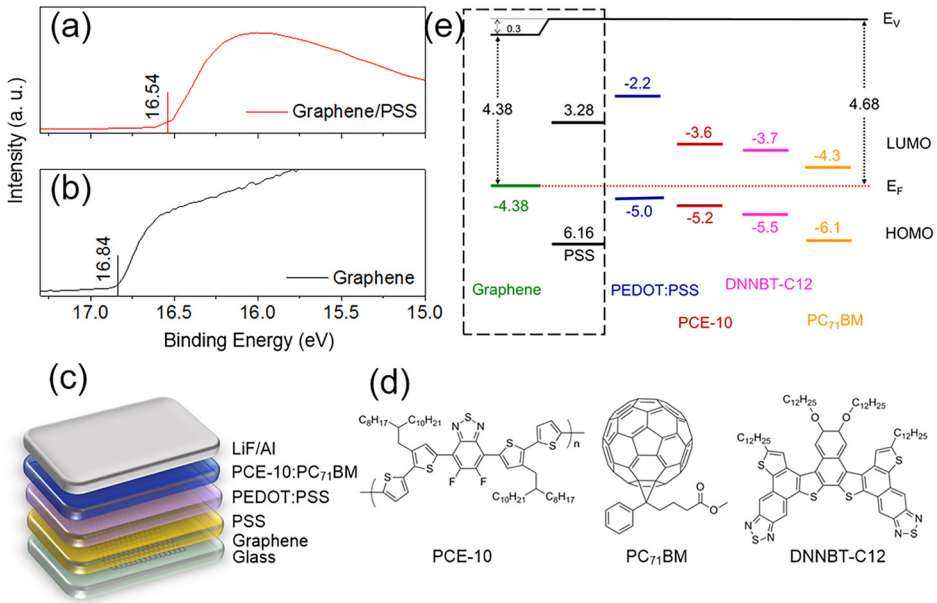

FIG. 2. Magnified UPS spectra of the photoemission cut-off of graphene (a) with and (b) without modification, (c) device configuration of OPV, (d) molecular structures of PCE-10, $PC_{71}BM$ and DNNBT-C12, and (e) corresponding energy level diagram of the as-fabricated OPV.

performances. The data summarized in Fig. 3(a) and Table I indicated that the PSS interfacial modification not only slightly alters the V_{oc} value but also obviously enhances J_{sc} and FF from 12.27 mA/cm^2 and 36.4% (device 1) to 15.42 mA/cm^2 and 44.6% (device 2), with a resulting PCE of 5.35% (device 2). The control device (device 1) showed an extremely low PCE and FF mainly owing to a large sheet resistance of the pristine graphene (1 kΩ/sq), which resulted in a large series resistance inside the solar cell. Moreover, the mismatch of graphene's WF and the highest occupied molecular orbital (HOMO) of PEDOT:PSS made charge extraction at the PEDOT:PSS/MLG interface difficult, thus followed by a low FF.[23] This situation was improved by coating another PSS interfacial modification layer onto graphene to form an interfacial dipole. As shown in Fig. 2(e), the bending of HOMO and vacuum level made hole extraction easier due to a decreased energy barrier for hole carriers, with which an overall improvement on J_{sc}, FF, and PCE was observed, as the statistical distributions of more than 15 devices shown in panels (f), (g), and (h) of Fig. 3. It was furthermore demonstrated by external quantum efficiency (EQE) curves [Fig. 3(c)] with significant enhancements over the entire visible region in device 2. More importantly, the PSS-modified devices exhibited a comparative stability to those unmodified ones when they were tested in a glove box under an accelerated aging condition with a continuous AM1.5G illumination [Fig. S2(a) in the supplementary material; the unencapsulated devices were measured at 32 °C], which was primarily because the PSS interfacial modification did not cause MLG stability issues such as chemical doping,[24] and the sheet resistance of our graphene showed a negligible change with storage time, as shown in Fig. S2(b) (supplementary material).

In order to obtain more efficient optoelectronic conversion efficiency, a small molecular material DNNBT-C12 [panel (d) of Fig. 2][19] was introduced into the PCE-10:$PC_{71}BM$ active layer to form a ternary blended polymer solar cell. With an optimized weight ratio of 2 wt. % for DNNBT-C12, a high PCE of 6.29% was acquired in the ternary OPVs after PSS modification (device 4), with typical parameters listed in Table I. To explain the influence of DNNBT-C12 on the photoactive layer and the device performance, the absorption spectra of

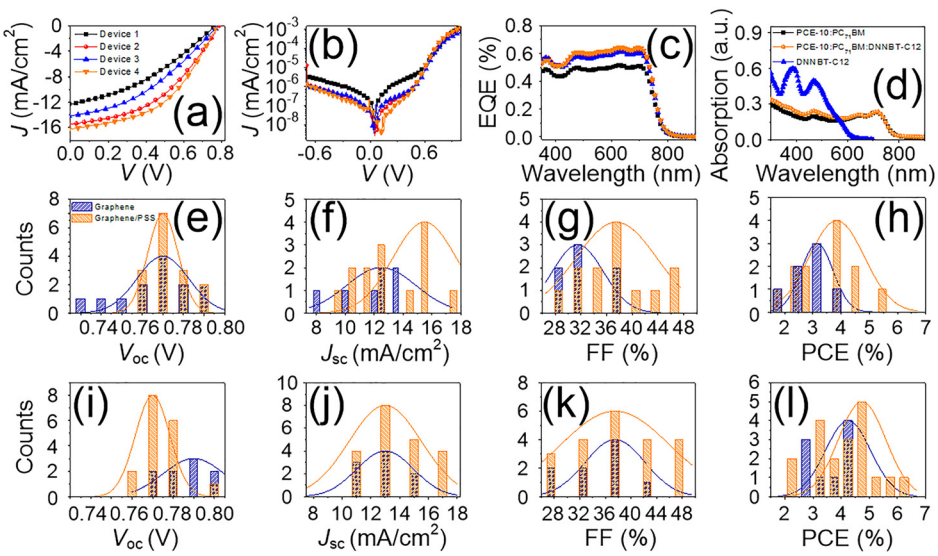

FIG. 3. Current-voltage characteristics (a) under AM 1.5G illumination and (b) dark conditions, (c) EQE curves of as-fabricated devices, and (d) the absorption spectra of the PCE-10:$PC_{71}BM$:DNNBT-C12 film and the control film without DNNBT-C12. The film absorption spectrum of DNNBT-C12 is also attached. The distribution histograms of parameters including (e) V_{oc}, (f) J_{sc}, (g) FF, and (h) PCE in PCE-10:$PC_{71}BM$-based devices composed of pristine graphene or modified graphene, while (i), (j), (k), and (l) show the distribution histograms of V_{oc}, J_{sc}, FF, and PCE in DNNBT-C12-doped PCE-10:$PC_{71}BM$ devices.

TABLE I. Summary of the photovoltaic parameters of the cells.

Cell Devices		V_{oc} (V)	J_{sc} (mA/cm^2)	FF (%)	PCE (%)
1	Control	0.77 (0.73–0.79)	12.27 (8.0–13.6)	36.4 (28.5–37.5)	3.42 (1.75–3.85)
2	PSS	0.78 (0.76–0.79)	15.42 (9.5–17.5)	44.6 (28.5–46.5)	5.35 (1.75–5.46)
3	DNNBT-C12	0.77 (0.77–0.80)	14.10 (11.0–15.0)	38.4 (27.5–42.5)	4.17 (2.75–4.25)
4	PSS and DNNBT-C12	0.77 (0.76–0.80)	16.15 (11.0–17.0)	47.8 (27.5–47.5)	6.29 (2.25–6.29)

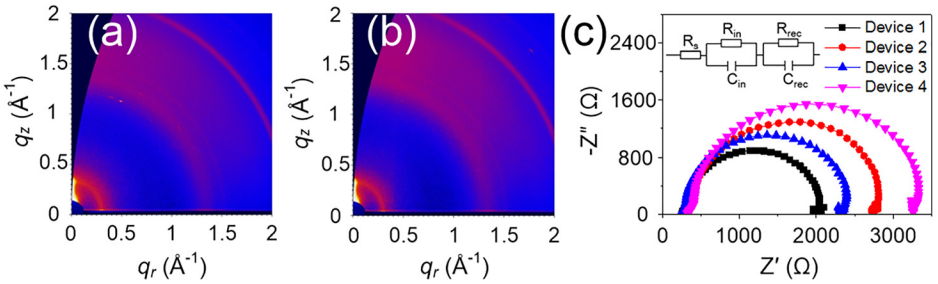

FIG. 4. The GIWAXS patterns of PCE-10:$PC_{71}BM$ thin films (a) without and (b) with DNNBT-C12. (c) Nyquist plots of devices 1–4 under dark conditions at an applied voltage of 0.6 V. The inset shows the equivalent circuit.

DNNBT-C12 [panel (d) of Fig. 3] and grazing incidence wide-angle X-ray scattering (GIWAXS) measurements of PCE-10:$PC_{71}BM$ with and without DNNBT-C12 [panels (a) and (b) of Fig. 4] were obtained. The intrinsic absorption of DNNBT-C12 at 300–650 nm induced a stronger absorption of the active layer in the visible region, thus enhancing the EQE. Scattering patterns for the active layer with and without DNNBT-C12 exhibited similar features with the PCE-10 (100) lamellar ring located at $q \approx 0.30$ Å^{-1} and $PC_{71}BM$ amorphous ring at $q \approx 1.3$ Å^{-1}. There were no obvious changes in scattering ring intensity, position, and width, which suggests that no significant molecular packing change was induced by DNNBT-C12 doping.[25]

To further understand the influence of PSS and DNNBT-C12 on the device performances, electrochemical impedance spectroscopy (EIS) measurements for the OPVs using different interfacial modification layers and active layers were carried out with their Nyquist plots shown in Fig. 4(c). The spectra showing a large semicircle at low frequencies and additional minor features in the high-frequency part were fitted with two series RC circuits, as shown in the inset of Fig. 4(c). To clearly describe processes in the OPVs, the following factors below were used in the equivalent circuit model: R_s represents the series resistance consisting of ohmic components, while R_{in} and R_{rec} are resistance components forming a parallel circuit with the corresponding capacitances (C_{in} and C_{rec}) at those contact interfaces inside the devices. The high-frequency part of the spectra usually contains information of transport and series resistance elements, e.g., alteration of high-frequency resistance (R_{in}) with the use of dielectric materials.[26] Analysis indicated that R_{in}s in PSS-modified devices was 8.97 Ω cm^2 and 6.34 Ω cm^2 for devices 2 and 4, respectively, slightly larger than 5.76 Ω cm^2 (device 1) and 4.99 Ω cm^2 (device 3), which was primarily due to the insulated nature of PSS. It is interesting to note that a reduced R_{in} value at high frequency was observed when DNNBT-C12 was doped into the active layer. The arc observed at low frequency in the Nyquist plot of organic solar cells is often described with R_{rec}, associated with the recombination process at contact interfaces. The PSS-modified OPVs showed an obvious increase in R_{rec} (from 180.3 Ω cm^2 to 259.2 Ω cm^2), and this represented less recombination and sufficient dissociation of carriers in our OPVs with the use of PSS. Similarly, adding DNNBT-C12 into the PCE-10:$PC_{71}BM$ active layer generated an even higher R_{rec} of 309.0 Ω cm^2, indicating that the use of DNNBT-C12 not only enhanced the absorption of PCE-10:$PC_{71}BM$ but also reduced recombination inside the active layer. The high R_{rec}s in these OPVs with PSS and DNNBT-C12 resulted in an increased FF and thereby a high PCE.

In conclusion, an insulated polymer PSS was used to modify the graphene sheets, and then, this PSS-modified graphene was applied as OPV anodes. The PCE was significantly enhanced from 3.42% to 5.35% in a PCE-10:$PC_{71}BM$ bulk heterojunction OPV due to the increase in graphene's WF engineered with an ultrathin PSS interfacial dipole layer. Moreover, the PSS interfacial modification also improved the hydrophilic feature of graphene films and significantly enlarged the recombination resistance, which contributed to the homogeneous coating of the following layers on graphene and the reduced recombination of photogenerated excitons. In addition, another small molecular material DNNBT-C12 was doped into the PCE-10:$PC_{71}BM$ active layer to form a ternary blended OPV, and the PCE was increased up to 6.29% due to an improved light absorption of the active layer and a larger recombination resistance in devices. The interface modification technique and the ternary blended material reported in this work provide an efficient solution to enhance optoelectronic conversion efficiency in OPVs with graphene anodes.

See supplementary material for XPS C1s spectra of the graphene sheets and stability data of graphene films and OPVs.

The authors acknowledge financial support from the National Foundation for Science and Technology Development (973 project, Grant Nos. 2015CB932203 and 2017YFB0404501), the National Natural Science Foundation of China (Grant Nos. 61274065, 51203077, 51173081, 61675085, 21404058, 61136003, 61675085, 61322402, and BZ2010043), the

Ministry of Education of China (No. IRT1148), the Key Project of Chinese Ministry of Education (Grant Nos. 104246 and 707032), the Science Fund for Distinguished Young Scholars of Jiangsu Province of China (Grant No. BK20160039), the Natural Science Foundation of Jiangsu Province (Grant Nos. BM2012010 and SBK2017041570), the Priority Academic Program Development of Jiangsu Higher Education Institutions (Grant No. YX030002), the Jiangsu National Synergetic Innovation Center for Advanced Materials, the Synergetic Innovation Center for Organic Electronics and Information Displays, and the Open Foundation from Jilin University (Grant No. IOSKL2015KF32). J. M and X.L acknowledge the financial support from RGC of Hong Kong GRF (No. 14314216) and the beam time and technical supports provided by beamline 14B1 and 19U2 beamlines at Shanghai Synchrotron Radiation Facility.

[1]M. W. Rowell, M. A. Topinka, M. D. McGehee, H. J. Prall, G. Dennler, N. S. Sariciftci, L. B. Hu, and G. Grüner, Appl. Phys. Lett. **88**, 233506 (2006).
[2]J. van de Lagemaat, T. M. Barnes, G. Rumbles, S. E. Shaheen, T. J. Coutts, C. Weeks, I. Levitsky, J. Peltola, and P. Glatkowski, Appl. Phys. Lett. **88**, 233505 (2006).
[3]T.-H. Han, Y. Lee, M.-R. Choi, S.-H. Woo, S.-H. Bae, B. H. Hong, J.-H. Ahn, and T.-W. Lee, Nat. Photon. **6**, 105 (2012).
[4]L. Gomez De Arco, Y. Zhang, C. W. Schlenker, K. Ryu, M. E. Thompson, and C. W. Zhou, ACS Nano **4**, 2865 (2010).
[5]J.-Y. Lee, S. T. Connor, Y. Cui, and P. Peumans, Nano Lett. **8**, 689 (2008).
[6]F. Guo, X. D. Zhu, K. Forberich, J. Krantz, T. Stubhan, M. Salinas, M. Halik, S. Spallek, B. Butz, E. Spiecker, T. Ameri, N. Li, P. Kubis, D. M. Guldi, G. J. Matt, and C. J. Brabec, Adv. Energy Mater. **3**, 1062 (2013).
[7]G. Eda, Y. Y. Lin, S. Miller, C. W. Chen, W. F. Su, and M. Chhowalla, Appl. Phys. Lett. **92**, 233305 (2008).
[8]J. B. Wu, H. A. Becerril, Z. N. Bao, Z. F. Liu, Y. S. Chen, and P. Peumans, Appl. Phys. Lett. **92**, 263302 (2008).
[9]M. Choe, B. H. Lee, G. H. Jo, J. Park, W. J. Park, S. C. Lee, W.-K. Hong, M.-J. Seong, Y. H. Kahng, K. Lee, and T. Lee, Org. Electron. **11**, 1864 (2010).
[10]Y. Wang, X. H. Chen, Y. L. Zhong, F. R. Zhu, and K. P. Loh, Appl. Phys. Lett. **95**, 063302 (2009).
[11]Z. K. Liu, J. H. Li, Z. H. Sun, G. A. Tai, S. P. Lau, and F. Yan, ACS Nano. **6**, 810 (2012).
[12]Y. M. Shi, K. K. Kim, A. Reina, M. Hofmann, L. J. Li, and J. Kong, ACS Nano. **4**, 2689 (2010).
[13]G. H. Jo, S. I. Na, S. H. Oh, S. Lee, T. S. Kim, G. Wang, M. Choe, W. Park, J. Yoon, D. Y. Kim, and Y. H. Kahng, Appl. Phys. Lett. **97**, 213301 (2010).
[14]H. Park, J. A. Rowehl, K. K. Kim, V. Bulovic, and J. Kong, Nanotechnol. **21**, 505204 (2010).
[15]S. Lee, J.-S. Yeo, Y. Ji, C. Cho, D.-Y. Kim, S.-I. Na, B. H. Lee, and T. Lee, Nanotechnol. **23**, 344013 (2012).
[16]H. Wu, X. Y. Zhang, Y. Zhang, L. Yan, W. Z. Gao, T. Q. Zhang, Y. D. Wang, J. Zhao, and W. W. Yu, ACS Appl. Mater. Inter. **7**, 21082 (2015).
[17]K. Kim, S.-H. Bae, C. T. Toh, H. Kim, J. H. Cho, D. Whang, T.-W. Lee, B. Özyilmaz, and J.-H. Ahn, ACS Appl. Mater. Inter. **6**, 3299 (2014).
[18]R. Steim, S. A. Choulis, P. Schilinsky, and C. J. Brabec, Appl. Phys. Lett. **92**, 093303 (2008).
[19]X. Shi, S. L. Liu, C. M. Liu, Y. M. Hu, S. H. Shi, N. N. Fu, B. M. Zhao, Z. H. Wang, and W. Huang, Chem.-Asian J. **11**, 2188 (2016).
[20]C. L. Hsu, C. T. Lin, J. H. Huang, C. W. Chu, K. H. Wei, and L. J. Li, ACS Nano **6**, 5031 (2012).
[21]A. Das, S. Pisana, B. Chakraborty, S. Piscanec, S. K. Saha, U. V. Waghmare, K. S. Novoselov, H. R. Krishnamurthy, A. K. Geim, A. C. Ferrari, and A. K. Sood, Nat. Nanotechnol. **3**, 210 (2008).
[22]S. Sanders, A. Cabrero-Vilatela, P. R. Kidambi, J. A. Alexander-Webber, C. Weijtens, P. Braeuninger-Weimer, A. I. Aria, M. M. Qasim, T. D. Wilkinson, J. Robertson, S. Hofmann, and J. Meyer, Nanoscale **7**, 13135 (2015).
[23]H. Park, Y. M. Shi, and J. Kong, Nanoscale **5**, 8934 (2013).
[24]Y. P. Liu, E. Jung, Y. Wang, Y. Zheng, E. J. Park, S. M. Cho, and K. P. Loh, Small **10**, 944 (2014).
[25]J. Y. Hao, Y. Xu, S. F. Chen, Y. P. Zhang, J. Q. Mai, T. K. Lau, R. Zhang, Y. Mei, L. H. Wang, X. H. Lu, and W. Huang, Opt. Commun. **362**, 50 (2016).
[26]G. Garcia-Belmonte, P. P. Boix, J. Bisquert, M. Sessolo, and H. J. Bolink, Sol. Energy Mater. Sol. Cells **94**, 366 (2010).